International Journal of Heat and Mass Transfer 119 (2018) 922–930

Contents lists available at ScienceDirect

International Journal of Heat and Mass Transfer

journal homepage: www.elsevier.com/locate/ijhmt

Design of a heat exchanger working with organic nanofluids using multi-objective particle swarm optimization algorithm and response surface method

Mohammad Hemmat Esfe [a,*], Omid Mahian [b,c,*], Mohammad Hadi Hajmohammad [a], Somchai Wongwises [b,d]

[a] Department of Mechanical Engineering, Imam Hossein University, Tehran, Iran
[b] Fluid Mechanics, Thermal Engineering and Multiphase Flow Research Laboratory (FUTURE Lab.), Department of Mechanical Engineering, Faculty of Engineering, King Mongkut's University of Technology Thonburi, Bangmod, Bangkok 10140, Thailand
[c] Center for Advanced Technologies, Ferdowsi University of Mashhad, Mashhad, Iran
[d] The Academy of Sciences, Royal Society of Thailand, Sanam Suea Pa, Dusit, Bangkok 10300, Thailand

ARTICLE INFO

Article history:
Received 8 October 2017
Received in revised form 30 November 2017
Accepted 1 December 2017

Keywords:
Organic nanofluids
Heat exchanger design
Optimization
Swarm optimization algorithm
Response surface method

ABSTRACT

In this study, the Pareto optimal design of COOH-MWCNTs nanofluid was investigated to reduce pressure drop and increase the relative heat transfer coefficient. Objective function modeling was based on empirical data, the solid volume fraction, and Reynolds number and then simulated with the response surface method in Design Expert software. After the objective function approximation, the regression coefficient of more than 0.9 for this study indicated the high accuracy of modeling through the RSM. To implement the optimization process, the powerful multi-objective particle swarm optimization algorithm was used. To show the correct optimization process, the results of the first and last generations of optimization are presented at the Pareto front, with all parts of it being non-dominant and optimized. Optimal results showed that to achieve a minimum pressure drop, the relative solid volume fraction should be at the minimum interval, and to achieve the maximum heat transfer coefficient, the relative solid volume fraction should be at the maximum interval. In addition, all optimal parts have the Reynolds number in the maximum range. At last, the optimum locations are presented, and the designer can select from these optimal points.

1. Introduction

Increasing heat transfer and heat transfer fluids has been the subject of much research in recent decades. Heat transfer fluids provide conditions for energy exchange in a system, and their effects depend on physical properties, such as thermal conductivity, viscosity, density, and heat capacity. Low thermal conductivity is often the most important limitation of heat transfer fluids. Among the studies conducted to overcome this limitation, Choi's proposed approach for the distribution of nanoparticles in a base fluid and for making nanofluids can be described as the best solution [1]. The impact of nanoparticles on the thermal conductivity of fluids can have a direct effect on heat transfer performance, thus increasing the heat transfer coefficient of fluids [2–8].

According to studies, the increasing temperature and solid volume fraction of nanoparticles in fluids can be called two important factors increasing the thermal conductivity of nanofluids [9–19]. In a study that Hemmat Esfe and Saedodin [3] carried out, the heat transfer characteristics of MgO/water nanofluids were tested in a heat exchanger. The results showed that a nanofluid with a higher-volume fraction and with a lower diameter of its nanoparticles has a higher Nusselt number and therefore, the higher the heat transfer coefficient. To predict the behavior of the heat transfer coefficient, pressure drop, and thermodynamic properties, such as thermal conductivity and the viscosity of nanofluids that various factors influence, mathematical relationships can be used. However, recently, software techniques, such as neural networks, have been used for this purpose. In Table 1, some of the studies in the field of modeling neural networks can be seen (Refs. [20–28]).

In a study, Hemmat Esfe et al. [29] Investigated the viscosity of TiO_2/water nanofluids using a neural network design. The

* Corresponding authors at: Fluid Mechanics, Thermal Engineering and Multiphase Flow Research Laboratory (FUTURE Lab.), Department of Mechanical Engineering, Faculty of Engineering, King Mongkut's University of Technology Thonburi, Bangmod, Bangkok 10140, Thailand (O. Mahian).
E-mail addresses: omid.mahian@gmail.com, omid.mah@kmutt.ac.th (O. Mahian).

https://doi.org/10.1016/j.ijheatmasstransfer.2017.12.009
0017-9310/

Nomenclature

T	temperature (°C)
w	weight (gr)
k	thermal conductivity (W m^{-1} °C^{-1})
Re	Reynolds number
ANOVA	analysis of variance
MWCNT	Multi-Walled Carbon Nanotube
MOPSO	Multiple Objective Particle Swarm Optimization
MOO	multi-objective optimization
GA	Genetic algorithm
NSGA-II	non-dominated sorting genetic algorithm-II
RSM	Response surface methodology
DOE	Design of experiments

Greeks symbols

ρ	density (kg m^{-3})
φ	particle solid volume fraction

Subscripts

Nf	nanofluid
bf	base fluid

algorithm used was a multilayer perceptron, which contains a hidden layer and four neurons. The results showed the high power of neural networks in predicting the experimental data, with the calculated regression coefficient being equal to 0.9998. Optimization between different parameters that sometimes conflict with one another has become an important issue in engineering problems in the past decade. The process that optimizes the collection of functions is called multi-objective optimization (MOO). Contrary to single-objective modeling, in MO problems, the objective is a set of points. All of these points apply the Pareto optimality definition for an optimal result at the Pareto front [30]. In recent years, studies on the algorithms of development (EAs) increased to expand MOO methods. Among famous algorithms, the genetic algorithm (GA) and non-dominated sorting genetic algorithm-II algorithm (NSGA-II) can be named [24,31–34].

Response surface methodology (RSM) is a set of mathematical methods that determine the relationship between one or more response variables with several independent variables (studied). In engineering, many phenomena can be modeled based on their related theories. In the case of the ineffectiveness of other modeling, the use of empirical modeling may work, with one of the most important of them being RSM [35–37]. For instance, Hussein et al. [38] designed a test for two nanofluids' heat transfer—SiO_2/water and TiO_2/water—in the radiator of a car. The results showed an increase in heat transfer by increasing the volumetric flow rate, inlet temperature, and solid volume fraction of the nanoparticles. Finally, they considered temperature variables, the volumetric flow rate, and the solid volume fraction as inputs and the Nusselt number as the response and designed a model. Besides MOO and response surface methods, some other methods may be used to analysis the heat exchangers which are based on entropy generation method [39,40].

In this study, to increase the relative heat transfer coefficient, and the relative pressure drop reduction of the COOH_MWCNTs nanofluid, a powerful optimization algorithm called swarm multi-objective particle was used. The objective functions were approximated using experimental data and the RSM and as the output were provided functions as polynomial objective functions.

To implement process optimization, the obtained model for objective functions connected to the multi-objective particle swarm algorithm (birds), and at each assessment, objective functions were used. After the implementation of the optimization process, to observe the optimization process, the results of the optimization of two main objectives in the first and last generations were presented in the form of Pareto front.

In this study, to increase the relative heat transfer coefficient and to reduce the relative pressure drop of COOH_MWCNTs nanofluid, the powerful multi-objective particle swarm optimization (MOPSO) algorithm was used. The objective functions were approximated using the experimental data and the RSM, and polynomial functions are presented for objective functions as the outputs. To implement the optimization process, the obtained models for objective functions were put into the multi-objective particle swarm (birds) algorithm, and at each assessment, these objective functions were used. After running the optimization process, to observe it, the results of the two objective functions' optimization in the first and last generations were presented in the form of the Pareto front.

Table 1
A summary of the studies in the field of modeling a neural network of nanofluid properties.

Author(s)	Nanofluid	Target(s)	Regression quality	Algorithm
Hemmat Esfe et al. [20]	Fe/EG	Thermal conductivity Dynamic viscosity	MSE = 0.00016 MSE = 0.00026	MLP
Hemmat Esfe et al. [21]	Al_2O_3/water	Thermal conductivity	MSE = 2.42E−6	MLP
Adham et al. [22]	SiC/water TiO_2/water	Thermal resistance & pumping power		NSGA-II
Zhao et al. [23]	Al_2O_3/water CuO/water	Dynamic viscosity	R-squared = 0.9962 R-squared = 0.9998	RBF
Mehrabi et al. [24]	TiO_2/water	Nusselt number & Pressure drop	MAE = 0.835 MRE = 8.9% RMSE = 1.01	GA-PNN & GMDH & NSGA-II
Ziaei-Rad et al. [25]	Al_2O_3/water	Friction factor Nusselt number	MRE = 0.19% MRE = 0.36%	MLP
Meybodi et al. [26]	Al_2O_3/water TiO_2/water SiO_2/water CuO/water	Dynamic viscosity	R-squared = 0.998	LSSVM
Santra et al. [27]	CuO/water	Nusselt number	MRE = 2.54 STDR = 2.46%	RPROP
Sharifpur et al. [28]	Al_2O_3/glycerol	Dynamic viscosity	R-squared = 0.9905	GMDH

2. Simulation of the objective functions with RSM

In this study, to achieve an appropriate objective function for the experimental results, the RSM and Design Expert software were used.

2.1. Estimation of objective functions

2.1.1. DOE

DoE is the design of experiments which is an essential aspect of the RSM [41]. Initially, these schemes were established to fit the physical experiments, but now, it is also appropriate for numerical experiments. Choosing the points where the response should be assessed is the target of the DOE.

The mathematical model of the process is the prominent criterion for the optimal DOE. Because polynomials form these mathematical models with an indefinite structure, for a very particular problem, special experiments are designed. The choice of the DOE influences the precision of the approximation and the cost of creating the response surface.

Among books many researchers explained the detailed DOE theory [41–43]. Schoofs [42] studied the use of experimental design for fundamental optimization. In addition, Unal et al. [43] discussed the usage of several designs for the RSM and multidisciplinary design optimization. An experimental design was established via an individual combination of runs as shown in Section 3.1. The level for each independent variable is a setting in the N-dimensional space. In the next section, several methodologies are compared.

The RSM explores the optimum operating situations through experimental data. To provide the path in the next step, many experiments were conducted using the results of one experiment.

2.1.2. RSM

The RSM is a method for optimizing processes with great mathematical and statistical methods. The RSM can be used in a special situation where different inputs influence a measurement and in the assessment of a process based on quality characteristics. In a measurement process, the measured value is called the response, and the input variables are the independent variables that the engineers control. In this study, to enhance the proper estimation model for the measurement process, the statistical modeling aspect of the RSM was used. One statistical skill is multiple regressions, which can be used to build experimental models with the RSM. In relation (1), the first-order multiple regression model with two independent inputs is represented.

$$y = \beta_0 + \beta_1 x_1 + \beta_2 x_2 + \varepsilon \tag{1}$$

In the above equation, the β_0, β_1, and β_2 are unknown parameters. x_1 and x_2 are the independent inputs, which are called the predictor or regressor, and y is the target value. The unknown parameters are found with the least squares method to estimate predator coefficients β in the multiple linear regression model in Eq. (1).

The matrix form of the regression model is as follows.

$$Y = X\beta + \varepsilon \tag{2}$$

In this equation, Y is the target values in an n × 1 vector; X is the independent parameters in an n × p matrix; β is a regression coefficient in a p × 1 vector; and ε is a random error in an n × 1 vector.

Least squares estimators are a technique used to evaluate the accuracy of the linear regression model. In this model, the least squares method produces an unbiased estimation of β. The sum of the residuals is the prominent parameters represented below.

$$SS_E = \sum_{i=1}^{n}(y_i - \hat{y}_i)^2 = \sum_{i=1}^{n} e_i^2 = e^T e \tag{3}$$

The residual is the difference of measured value y_i from fitted value $\hat{y}_i$, which is defined as follows:

$$e_i = y_i - \hat{y}_i \tag{4}$$

Due to $X^T Xb = X^T y$, a computational equation for SSE can be deduced as follows:

$$SS_E = y^T y - b^T X^T y \tag{5}$$

The error or residual sum of squares is called Eq. (5).

σ^2 as the unbiased estimator is drawn as follows:

$$\sigma^2 = \frac{SS_E}{n-p} \tag{6}$$

where n is the measurement number and p is the regression coefficient. The total sum of squares is as follows:

$$SS_T = y^T y - \frac{\left(\sum_{i=1}^{n} y_i\right)^2}{n} = \sum_{i=1}^{n} y_i^2 - \frac{\left(\sum_{i=1}^{n} y_i\right)^2}{n} \tag{7}$$

Then, the multiple determination coefficients R^2 is defined as follows:

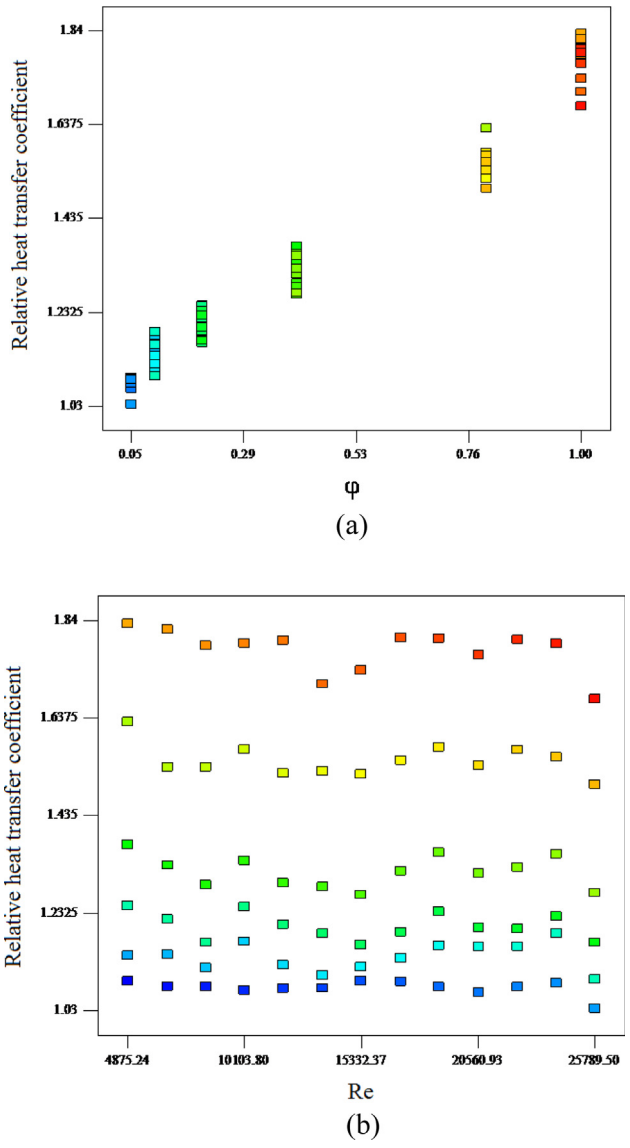

Fig. 1. Input data for relative heat transfer coefficient in terms of (a) concentration (b) Reynolds number.

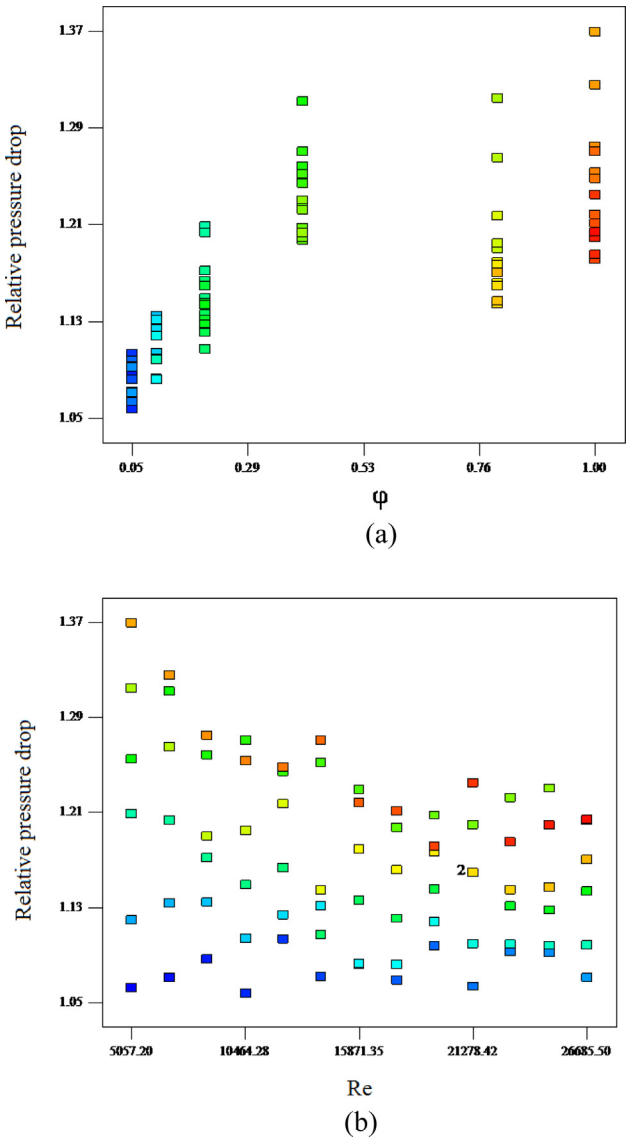

Fig. 2. Input data for relative pressure drop in terms of (a) concentration (b) Reynolds number.

$$R^2 = 1 - \frac{SS_E}{SS_T} \tag{8}$$

R^2 represents the reduction of y extracted with regressor variable X_k in the model. Investigating the Eq. (8) shows that $0 \le R^2 \le 1$. On the other hand, the large value of R^2 does not infer the accuracy of the regression model. To increase R^2, a variable can be added to the model, whether or not this variable is necessary statistically. Usually, much larger values of R^2 do not indicate the strength prediction of a new measurement or the estimation of the mean response.

Due to the malfunctioning of R^2, the researchers preferred to use an adjusted statistic version of R^2 as follows:

$$R^2_{adj} = 1 - \frac{SS_E/(n-p)}{SS_T/(n-1)} = 1 - \frac{n-1}{n-p}(1-R^2) \tag{9}$$

In fact, the adjusted R^2 statistic does not change by adding variables to the model. In addition, R^2_{adj} will often decrease by adding excessive parameters. This is the best way in which to add unnecessary variables in the model without changing the R^2 significantly [40].

The regression sum of squares always increases, and the error sum of squares decreases due to adding more variables to the regression model. Adding an external variable to the model continues until one decides that the result will feature good accuracy. Actually, the effectiveness of the model will decrease with adding further insignificant variables because this increases the mean square error [41,42].

Then, the cubic regression was used to analyze the response variables, and the best fitting mathematical models were determined. Furthermore, the regression model was compared with analysis of variance (ANOVA) to be sure about the adequacy of the model.

To approximate the functions using Design Expert software, the relative heat transfer coefficient and relative pressure drop of nanofluids were determined by testing them based on various quantities of the solid volume fraction of nanoparticles and the Reynolds number. The values of the heat transfer coefficient and the relative pressure drop in terms of the solid volume fraction and Reynolds numbers in different tests are presented in Figs. 1(-a, -b) and 2(-a, -b) respectively.

After modeling with RSM, relations (9) and (10) represent the functions of the heat transfer coefficient and the relative pressure drop of nanofluids based on the solid volume fraction of the nanoparticle and Reynolds number:

$$\begin{aligned}\text{Relative heat transfer coefficient} &= 0.98544 + 1.204\varphi + 1.493\text{E}-05Re - 4.41\text{E}-06\varphi Re \\ &\quad - 2.04194\varphi^2 - 1.33\text{E}-09Re^2 + 1.125\varphi^3 + 3.136\text{E}-14Re^3\end{aligned} \tag{10}$$

$$\begin{aligned}\text{Relative pressure drop} &= 1.233 + 1.215\varphi - 5.052\text{E}-05Re \\ &\quad - 2.548\text{E}-06\varphi Re - 1.592\varphi^2 \\ &\quad + 3.568\text{E}-09Re^2 + 1.166\varphi^3 \\ &\quad - 7.55\text{E}-14Re^3\end{aligned} \tag{11}$$

Table 2
Analysis of variance (ANOVA) for Relative heat transfer coefficient.

Source	DF	Adj SS	Adj MS	F	P
Model	7	4.73	0.68	1010.60	<.0001
A-φ	1	0.20	0.20	300.65	<.0001
B-*Re*	1	9.268E−03	9.268E−003	13.85	.0004
AB	1	2.761E−03	2.761E−003	4.13	.0460
A^2	1	0.028	0.028	42.00	<.0001
B^2	1	9.815E−04	9.815E−004	1.47	.2299
A^3	1	0.047	0.047	70.05	<.0001
B^3	1	0.020	0.020	29.51	<.0001
Residual error	70	0.047	6.692E−004		
Total	77	4.78			

Standard deviation = 0.026.
Predicted residual error of sum of squares (PRESS) = 0.059.
R^2 (Adequate) = 93.908% R^2 (Predicted) = 98.76% R^2 (Adjusted) = 99.02%.

Table 3
Analysis of variance (ANOVA) for Relative pressure drop.

Source	DF	Adj SS	Adj MS	F	P
Model	7	0.33	0.048	57.56	<.0001
A-φ	1	5.681E−003	5.681E−003	6.84	.0109
B-*Re*	1	0.041	0.041	48.90	<.0001
AB	1	0.012	0.012	14.86	.0003
A^2	1	0.034	0.034	40.87	<.0001
B^2	1	3.415E−003	3.415E−003	4.11	.0463
A^3	1	0.044	0.044	52.60	<.0001
B^3	1	0.016	0.016	19.21	<.0001
Residual error	70	0.058	8.301E−004		
Total	77	0.39			

Standard deviation = 0.029.
Predicted residual error of sum of squares (PRESS) = 0.076.
R^2 (Adequate) = 87.766% R^2 (Predicted) = 90.62% R^2 (Adjusted) = 95.20%.

After the modeling process with experimental data, the ANOVA results via the RSM in Design Expert software are provided for the heat transfer coefficient and relative pressure drop functions in Tables 2 and 3 respectively. The experimental data of the solid volume fraction of nanoparticles are in the range of 1–5%, and the experimental data of Reynolds are defined in the range of 26,680–4875.

2.1.3. ANOVA

The cubic models were examined with ANOVA statistically. Some results of ANOVA for the cubic model of the heat transfer coefficient are shown in Table 2. The importance of the regression model can be derived from the large F value of 1010.60. P-values infer the statistical aspect of the model, where values of less than .05 denote the significance of this aspect, and it should be less important for P-values of more than .05. Thus, the unimportant parts of the model are omitted.

The standard deviation of expenditure in the cubic model is listed in Table 3. No relation really exists between the expenditure function and *Re*. The expenditure model is shown with φ and dp. The large value of R^2, about 0.952, indicates the effectiveness of the expenditure regression model. This means the cubic model cannot estimate just 0.48% of the total variance with proper accuracy.

The R^2_{adj} value for efficiency and the cost of nanofluids in the above relations are 0.9902 and 0.9520 respectively. It should be noted that R^2_{adj} indicates the quality of the output function; the closer to 1, the greater the accuracy of these relations.

After modeling objective functions with the RSM, to assess the quality of these model functions, the regression graph of Design Expert software results based on experimental results for the heat transfer coefficient and relative pressure drop functions is presented in Fig. 3(-a) and (-b) respectively.

The above graphs compare the results of experimental data and predicted results via the RSM. According to the above diagrams, coincidence of modeling results on the actual value (line bisect), show the accuracy of the software.

The normal probability graphs of the residuals for thermal conductivity and viscosity have been displayed in Fig. 4(-a) and (-b) respectively.

A three-dimensional graph of the response surface of the heat transfer coefficient and relative pressure drop in terms of designing the Reynolds number and solid volume fraction of nanoparticles is shown in Fig. 5(-a) and (-b) respectively.

Then, to continue the optimization process, the multi-objective particle swarm algorithms, one of the most powerful methods for MOO, was used.

3. Optimization of nanofluid using MOPSO

MOPSO is an innovative search method that simulates the movements of a batch of birds looking for food.

3.1. MOPSO optimization method

The particle swarm optimization method is a smart direct search method. Like other smart methods, this method generates an initial population randomly; the members of this population are called

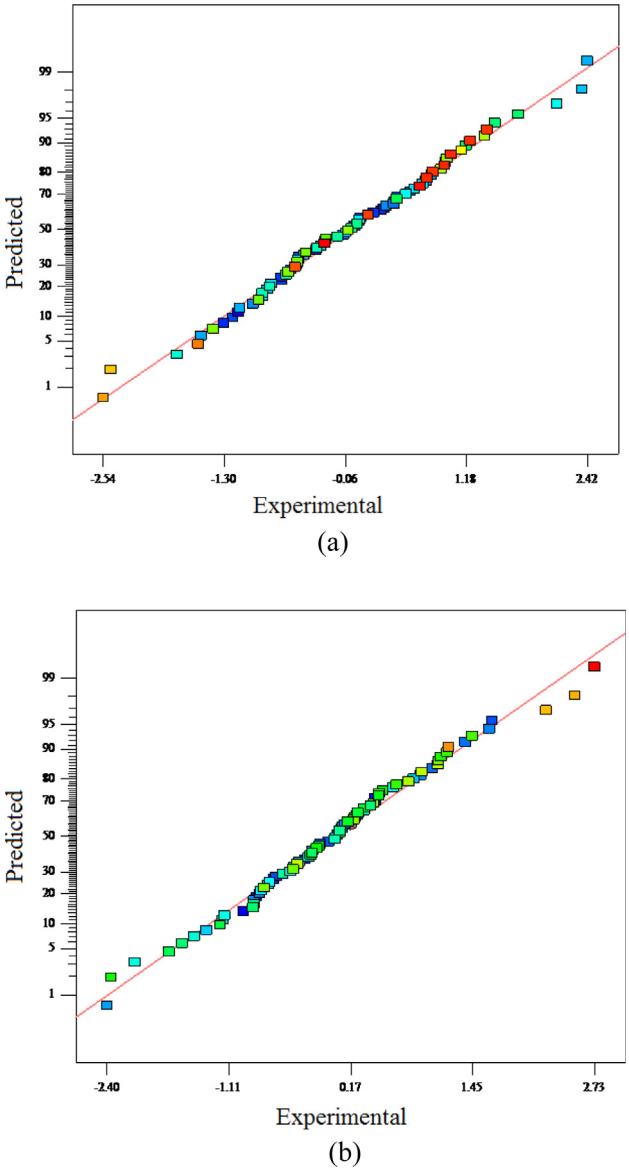

Fig. 3. Comparison of the experimental results and predicted values (a) Relative heat transfer coefficient (b) Relative pressure drop.

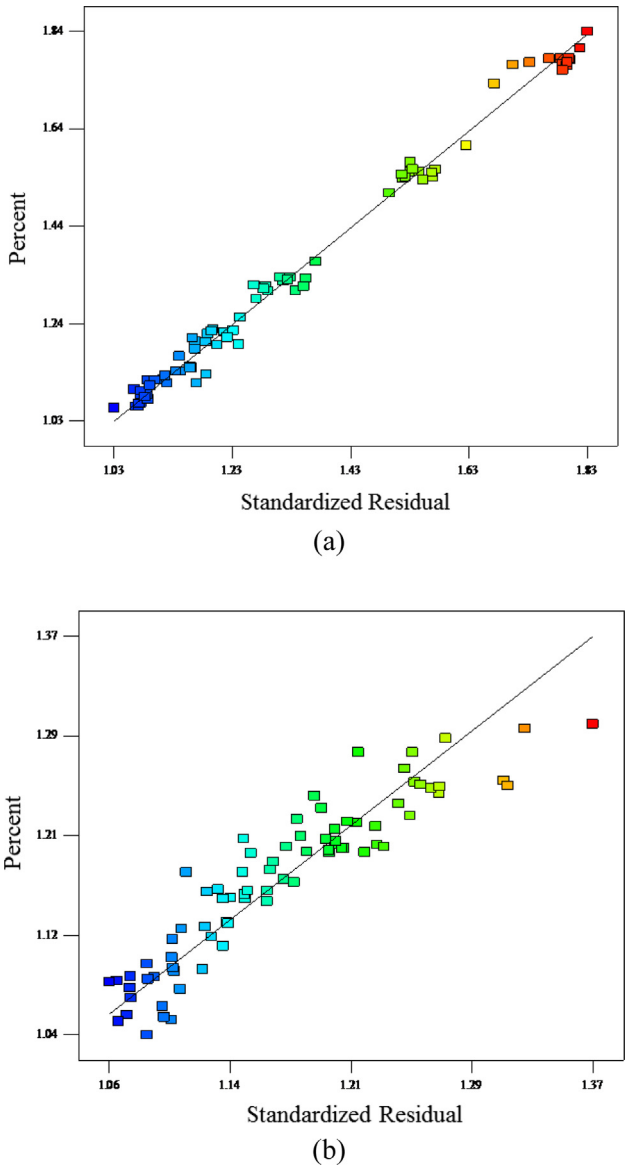

Fig. 4. Normal probability plot residuals. (a) Relative heat transfer coefficient (b) Relative pressure drop.

particles. In this algorithm, for each particle, a velocity vector is defined. Particles move to a better area during this process in the search space at velocities that dynamically adjust to their previous behavior. In the particle swarm optimization method, particles move across the multi-dimensional search space. The location of each particle is changed in accordance with its experience and its neighbors', too.

Suppose $\vec{x}(t)$ shows the position of particle I at time t. The next position is determined by adding speed to the position of particle I at time t. So Eq. (12) shows the next position.

$$\vec{x}_i(t+1) = \vec{x}_i(t) + \vec{v}_i(t+1) \tag{12}$$

In MOPSO, usually non-dominant responses are stored in a different location from the generation, called an external archive. This process is different in the NSGA-II. Thus, the external archive is a repository of non-dominant responses.

3.2. General trend of MOPSO algorithms

First, the initial population takes shape in the algorithm. In the first iteration, a set of best practices is defined with regard to the

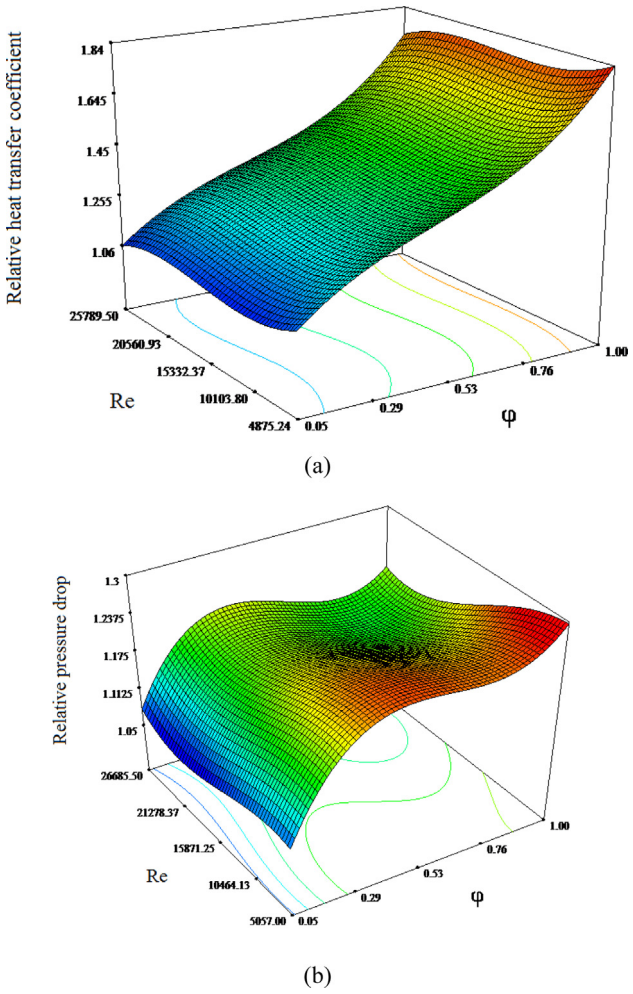

Fig. 5. Three-dimensional response surface graphs of (a) Relative heat transfer coefficient (b) Relative pressure drop.

non-dominant group of some particles to other particles in the population, and this set creates external archives. Then, the best group experience is chosen by using some qualitative measurement methods for each particle. In this paper, the networking method was used. At each iteration the best group experience for every practice is chosen and moves according to Eq. (12) that shows the next position. Then, in the new position of the particle, the objective function value is calculated, and the best personal experience is updated. If the new position of the particle is better than the best personal experience of it, or if both of them are the same, the new position is determined as the best personal experience. After updating the particles, the archive will be updated, and best practices will be determined. This process is repeated to satisfy the completed condition. Fig. 6 shows the structure of the MOPSO algorithm.

4. Results and discussion

In this study, the heat transfer coefficient and relative pressure drop functions were like objective functions and solid volume fractions and were used as design variables along with the Reynolds number. The objective functions were approximated using experimental data and via the RSM with the regression coefficient of above 0.9. To implement optimization, the powerful MOPSO algorithm with an initial population of 30 was used, and the archive member numbers of 30 and 50 repetitions were used. Modeled functions were attached to the particle swarm algorithm and were

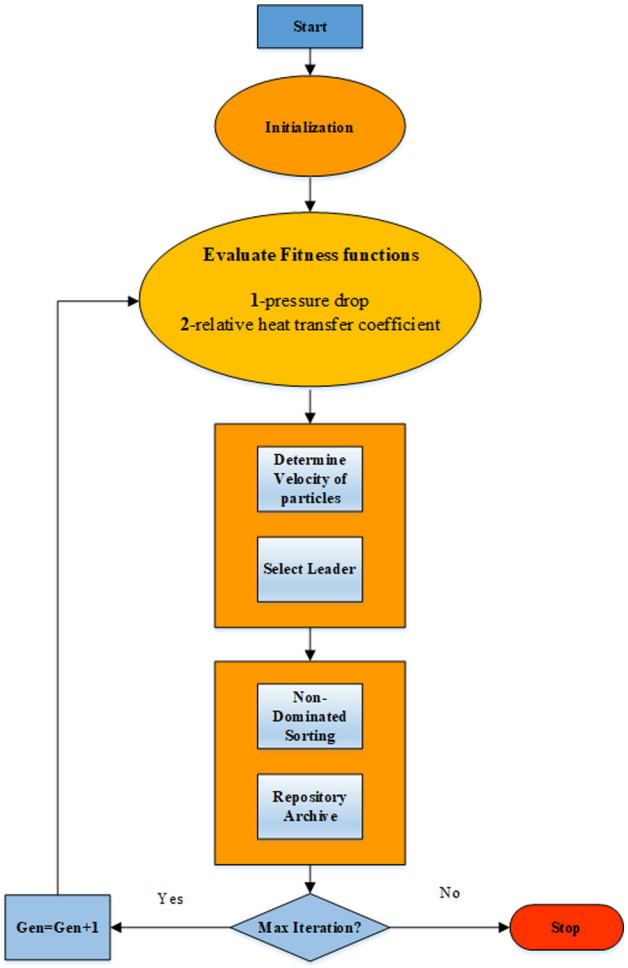

Fig. 6. Structure of MOPSO.

called in any evaluation of objective functions. After running the two-target optimization process, a set of non-dominant results at the Pareto front were obtained and are provided in Fig. 7. It should be noted that all of the results were optimized and non-dominant. In addition, in this figure, the results of the first front and final Pareto front of optimization are provided to compare the optimization process.

The above graph shows that the results of the last generation are more efficient and beat the results of the first generation, indicating the accuracy of the optimization process. It can be deduced from the Pareto front of the last generation that some part of the Pareto front shown between the dotted lines is not an optimum point. In this part, the relative heat transfer coefficient is in the range of 1:21 to 1:54, and the relative pressure drop is about 1.16. The experimental data extracted from Figs. 1 and 2 show that the input data for simulating the objective functions for the relative heat transfer coefficient values in the range of 1:21–1:54 contain a relative pressure drop higher than 1.2. These points are placed at the top of the Pareto front, which means the optimized Pareto front points have been defeated. Thus, these points have been removed in the optimization process, and no optimal points are present in this section.

It should be mentioned that all parts at the Pareto front end are non-dominant, and designers can choose each of them according to their needs. In MOO, usually one of the Pareto points is chosen as a compromise point. In fact, the compromise point is a balance between the values of objective functions, and a designer can

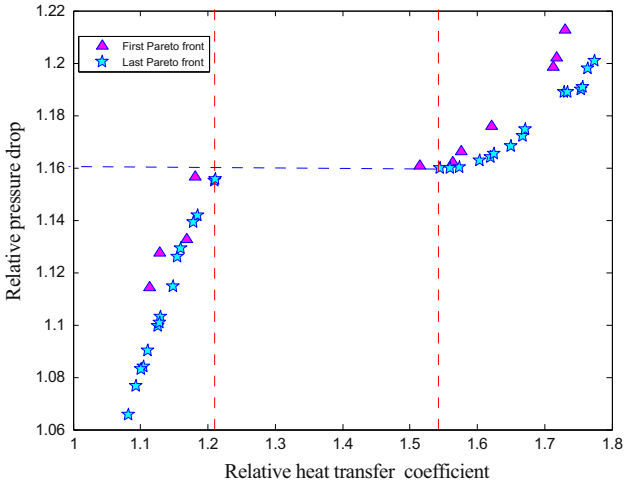

Fig. 7. Pareto Front of Optimization by MOPSO.

choose one of the Pareto front points in accordance with design requirements and the value of the objective function for targets. Thus, the characteristics and values of the Pareto front end points from the two-target optimization process specified in Fig. 6 are presented in Table 4. The final choice depends on the importance of each of the functions.

As it is clear from the results of the Table 4, to achieve the minimum relative pressure drop, the solid volume fraction should be in the minimum range (i.e., 0.05), and to achieve the maximum relative heat transfer coefficient, the solid volume fraction should be in the maximum range (close to 1). In addition, to reach the optimal points, the values of the Reynolds number should be near its maximum range (between 16,100 and 22,200).

Table 4
Optimum points of the multi-objective optimization By MOPSO.

φ	Re	Relative heat transfer coefficient	Relative pressure drop
0.9185	19745.43	1.667	1.1722
0.9032	20355.91	1.6496	1.168
0.8024	22154.69	1.5447	1.1596
0.9852	19938.3	1.7536	1.1899
0.8351	22123.57	1.573	1.1602
0.9215	19081.02	1.671	1.1746
0.9874	19939.73	1.7566	1.1907
1	18321.31	1.7739	1.2006
0.0712	16626.51	1.10519	1.0841
0.127	16434.22	1.1545	1.126
0.1569	17876.11	1.1845	1.141
0.05	16295.57	1.0822	1.0657
0.061	16158.29	1.0935	1.076
0.091	17138.16	1.126	1.0994
0.186	19303.34	1.2103	1.1549
0.0785	16414.78	1.1109	1.0902
0.095	16943.68	1.1295	1.103
0.0928	17168.76	1.1281	1.1007
0.0695	16126.43	1.1007	1.083
0.187	19349.26	1.211	1.1557
0.967	18442.8	1.728	1.1887
0.1515	17567.49	1.1789	1.139
0.1329	16542.72	1.1593	1.1292
0.8768	20904.42	1.6198	1.1638
0.9718	18723.92	1.734	1.1890
0.993	18338.92	1.7639	1.1979
0.8166	21460.34	1.5603	1.1598
0.8802	20191.16	1.6247	1.1652
0.1128	17735.92	1.1483	1.1146
0.8599	20571.93	1.603	1.1626

5. Conclusion

The aim of this work was the two-target optimization of COOH_MWCNTs nanofluids to increase the relative heat transfer coefficient and to decrease the relative pressure drop. The simulation of the target functions was done using experimental data and the RSM via Design Expert software. The obtained relation had high precision, and its regression coefficient was more than 0.9. MOPSO, the powerful multi-objective algorithm, was used for optimization. To implement an optimization process, the functions modeled with the RSM were connected to the MOPSO algorithm, and in each assessment, the objective functions were called. The results of the optimization were provided as Pareto fronts, where all points on it were optimized, and designers can choose between them according to their needs. Assessing the optimal Pareto front results showed that to achieve the minimum relative pressure drop, the solid volume fraction should be in the minimum range, and the maximum relative heat transfer coefficient was achieved in the maximum range of the solid volume fraction. In addition, all of the optimal points had Reynolds numbers in the range of 16,100 to 22,200 (close to the maximum Reynolds number).

Conflict of interest

There is no conflict of interest for this paper.

Acknowledgment

The fourth author acknowledges the financial support provided by the "Research Chair Grant" National Science and Technology Development Agency (NSTDA), the Thailand Research Fund (TRF) and King Mongkut's University of Technology Thonburi through the "KMUTT 55th Anniversary Commemorative Fund". The second author would like to thank the postdoc fellowship granted by KMUTT.

Appendix A. Supplementary material

Supplementary data associated with this article can be found, in the online version, at https://doi.org/10.1016/j.ijheatmasstransfer.2017.12.009.

References

[1] S.U.S. Choi, J.A. Eastman, Enhancing Thermal Conductivity of Fluids With Nanoparticles, Mater. Sci. 231 (1995) 99–105.
[2] M. Hemmat Esfe, S. Saedodin, O. Mahian, S. Wongwises, Thermophysical properties, heat transfer and pressure drop of COOH-functionalized multi walled carbon nanotubes/water nanofluids, Int. Commun. Heat Mass Transfer 58 (2014) 176–183.
[3] M. Hemmat Esfe, S. Saedodin, Turbulent forced convection heat transfer and thermophysical properties of Mgo–water nanofluid with consideration of different nanoparticles diameter, an empirical study, J. Therm. Anal. Calorim. 119 (2) (2015) 1205–1213.
[4] J. Cai, X. Hu, B. Xiao, Y. Zhou, W. Wei, Recent developments on fractal-based approaches to nanofluids and nanoparticle aggregation, Int. J. Heat Mass Transfer 105 (2017) 623–637.
[5] M. Hemmat Esfe, A. Karimipour, W.-M. Yan, M. Akbari, M.R. Safaei, M. Dahari, Experimental study on thermal conductivity of ethylene glycol based nanofluids containing Al2O3 nanoparticles, Int. J. Heat Mass Transfer 88 (2015) 728–734.
[6] M. Hemmat Esfe, A. Naderi, M. Akbari, M. Afrand, A. Karimipour, Evaluation of thermal conductivity of COOH-functionalized MWCNTs/water via temperature and solid solid volume fraction by using experimental data and ANN methods, J. Therm. Anal. Calorim. 121 (3) (2015) 1273–1278.
[7] D. Huang, Z. Wu, B. Sunden, Effects of hybrid nanofluid mixture in plate heat exchangers, Exp. Therm. Fluid Sci. 72 (2016) 190–196.
[8] O. Mahian, A. Kianifar, S.Z. Heris, D. Wen, A.Z. Sahin, S. Wongwises, Nanofluids effects on the evaporation rate in a solar still equipped with a heat exchanger, Nano Energy 36 (2017) 134–155.
[9] M. Hemmat Esfe, W.-M. Yan, M. Akbari, A. Karimipour, M. Hassani, Experimental study on thermal conductivity of DWCNT-ZnO/water-EG nanofluids, Int. Commun. Heat Mass Transfer 68 (Nov. 2015) 248–251.
[10] M. Hemmat Esfe, S. Saedodin, O. Mahian, S. Wongwises, Efficiency of ferromagnetic nanoparticles suspended in ethylene glycol for applications in energy devices: Effects of particle size, temperature, and concentration, Int. Commun. Heat Mass Transfer 58 (Nov. 2014) 138–146.
[11] M. Hemmat Esfe et al., Experimental investigation and development of new correlations for thermal conductivity of CuO/EG–water nanofluid, Int. Commun. Heat Mass Transfer 65 (2015) 47–51.
[12] A.M. Khdher, N.A.C. Sidik, W.A.W. Hamzah, R. Mamat, An experimental determination of thermal conductivity and electrical conductivity of bio glycol based Al2O3 nanofluids and development of new correlation, Int. Commun. Heat Mass Transfer 73 (Apr. 2016) 75–83.
[13] M. Xing, J. Yu, R. Wang, Experimental investigation and modelling on the thermal conductivity of CNTs based nanofluids, Int. J. Therm. Sci. 104 (Jun. 2016) 404–411.
[14] O. Mahian, A. Kianifar, S.Z. Heris, S. Wongwises, Natural convection of silica nanofluids in square and triangular enclosures: theoretical and experimental study, Int. J. Heat Mass Transfer 99 (2016) 792–804.
[15] M.H. Esfe, S. Esfandeh, S. Saedodin, H. Rostamian, Experimental evaluation, sensitivity analyzation and ANN modeling of thermal conductivity of ZnO-MWCNT/EG-water hybrid nanofluid for engineering applications, Appl. Therm. Eng. 125 (2017) 673–685.
[16] M.H. Esfe, S. Esfandeh, M. Rejvani, Modeling of thermal conductivity of MWCNT-SiO_2 (30: 70%)/EG hybrid nanofluid, sensitivity analyzing and cost performance for industrial applications, J. Therm. Anal. Calorim. (2017), https://doi.org/10.1007/s10973-017-6680-y.
[17] M. Amani, P. Amani, A. Kasaeian, O. Mahian, S. Wongwises, Thermal conductivity measurement of spinel-type ferrite $MnFe_2O_4$ nanofluids in the presence of a uniform magnetic field, J. Mol. Liquids 230 (2017) 121–128.
[18] M.H. Esfe, P. Razi, M.H. Hajmohammad, S.H. Rostamian, W.S. Sarsam, A.A.A. Arani, M. Dahari, Optimization, modeling and accurate prediction of thermal conductivity and dynamic viscosity of stabilized ethylene glycol and water mixture Al 2 O 3 nanofluids by NSGA-II using ANN, Int. Commun. Heat Mass Transfer 82 (2017) 154–160.
[19] M.H. Esfe, A. Alirezaie, M. Rejvani, TTTd alterations gradient of thermal conductivity increases with the rise of volume fraction of up to 1%, and emmmy then, the sensitivity decreases. Generally, the current study is a combination of empirical studies along, Appl. Therm. Eng. 111 (2017) 1202–1210.
[20] M. Hemmat Esfe, S. Saedodin, N. Sina, M. Afrand, S. Rostami, Designing an artificial neural network to predict thermal conductivity and dynamic viscosity of ferromagnetic nanofluid, Int. Commun. Heat Mass Transfer 68 (2015) 50–57.
[21] M. Hemmat Esfe, M. Afrand, W.-M. Yan, M. Akbari, Applicability of artificial neural network and nonlinear regression to predict thermal conductivity modeling of Al2O3–water nanofluids using experimental data, Int. Commun. Heat Mass Transfer 66 (2015) 246–249.
[22] A. Adham, N. Mohd-Ghazali, R. Ahmad, Optimization of nanofluid-cooled microchannel heat sink, Therm. Sci. 20 (1) (2016) 109–118.
[23] N. Zhao, X. Wen, J. Yang, S. Li, Z. Wang, Modeling and prediction of viscosity of water-based nanofluids by radial basis function neural networks, Powder Technol. 281 (2015) 173–183.
[24] M. Mehrabi, M. Sharifpur, J.P. Meyer, Modelling and multi-objective optimisation of the convective heat transfer characteristics and pressure drop of low concentration TiO2–water nanofluids in the turbulent flow regime, Int. J. Heat Mass Transfer 67 (2013) 646–653.
[25] M. Ziaei-Rad, M. Saeedan, E. Afshari, Simulation and prediction of MHD dissipative nanofluid flow on a permeable stretching surface using artificial neural network, Appl. Therm. Eng. (2016).
[26] M.K. Meybodi, S. Naseri, A. Shokrollahi, A. Daryasafar, Prediction of viscosity of water-based Al2O3, TiO2, SiO2, and CuO nanofluids using a reliable approach, Chemom. Intell. Lab. Syst., 149 (2015) 60–69.
[27] A.K. Santra, N. Chakraborty, S. Sen, Prediction of heat transfer due to presence of copper–water nanofluid using resilient-propagation neural network, Int. J. Therm. Sci. 48 (7) (2009) 1311–1318.
[28] M. Sharifpur, S.A. Adio, J.P. Meyer, Experimental investigation and model development for effective viscosity of Al2O3-glycerol nanofluids by using dimensional analysis and GMDH-NN methods, Int. Commun. Heat Mass Transfer 68 (Nov. 2015) 208–219.
[29] M.H. Esfe, M.R.H. Ahangar, M. Rejvani, D. Toghraie, M.H. Hajmohammad, Designing an artificial neural network to predict dynamic viscosity of aqueous nanofluid of TiO_2 using experimental data, Int. Commun. Heat Mass Transfer 75 (2016) 192–196.
[30] K. Deb, Multi-Objective Optimization Using Evolutionary Algorithms, John Wiley & Sons, Chichester, England, 2001.
[31] Y.-T. Yang, H.-W. Tang, W.-P. Ding, Optimization design of micro-channel heat sink using nanofluid by numerical simulation coupled with genetic algorithm, Int. Commun. Heat Mass Transfer 72 (Mar. 2016) 29–38.
[32] G.-M. Normah, J.-T. Oh, N.B. Chien, K.-I. Choi, A. Robiah, Comparison of the optimized thermal performance of square and circular ammonia-cooled microchannel heat sink with genetic algorithm, Energy Convers. Manag. 102 (Sep. 2015) 59–65.
[33] M. Amani, P. Amani, O. Mahian, P. Estellé, Multi-objective optimization of thermophysical properties of eco-friendly organic nanofluids, J. Clean. Prod. 166 (2017) 350–359.

[34] M. Hemmat Esfe, H. Hajmohammad, D. Toghraie, H. Rostamian, O. Mahian, S. Wongwises, Multi-objective optimization of nanofluid flow in double tube heat exchangers for applications in energy systems, Energy 137 (2017) 160–171.
[35] L. Sun, C.-L. Zhang, Evaluation of elliptical finned-tube heat exchanger performance using CFD and response surface methodology, Int. J. Therm. Sci. 75 (2014) 45–53.
[36] J.S. Nam, D.H. Kim, H. Chung, S.W. Lee, Optimization of environmentally benign micro-drilling process with nanofluid minimum quantity lubrication using response surface methodology and genetic algorithm, J. Clean. Prod. 102 (2015) 428–436.
[37] M. Rahimi-Gorji, O. Pourmehran, M. Hatami, D.D. Ganji, Statistical optimization of microchannel heat sink (MCHS) geometry cooled by different nanofluids using RSM analysis, Eur. Phys. J. Plus 130 (2) (2015) 22.
[38] A.M. Hussein, R.A. Bakar, K. Kadirgama, K.V. Sharma, Heat transfer enhancement using nanofluids in an automotive cooling system, Int. Commun. Heat Mass Transfer 53 (2014) 195–202.
[39] Z. Zhang, C. Jiang, Y. Zhang, W. Zhou, B. Bai, Virtual entropy generation (VEG) method in experiment reliability control implications for heat exchanger measurement, Appl. Therm. Eng. 110 (2017) 1476–1482.
[40] Z. Zhang, The Monte Carlo based virtual entropy generation analysis, Appl. Therm. Eng. 126 (Nov. 2017) 915–919.
[41] G.E.P. Box, N.R. Draper, Empirical Model Building and Response Surfaces, in: Empirical Model Building and Response Surfaces, vol. 30, no. 2, 1987, p. 74 and 424.
[42] A.J.G. Schoofs, Experimental design and structural optimization, in: Structural Optimization, Springer Netherlands, Dordrecht, 1988, pp. 307–314.
[43] R. Unal, R.D. Braun, A.A. Moore, R.A. Lepsch, Response Surface Model Building Using Orthogonal Arrays for Computer Experiments, NASA Langley Technical Report Server, 1997.